



# Position and cadence tracking of a motorized FES-cycle with an unknown time-varying input delay using saturated FES control<sup>☆</sup>

Brendon C. Allen<sup>a,\*</sup>, Kimberly J. Stubbs<sup>b</sup>, Warren E. Dixon<sup>b</sup>

<sup>a</sup> Department of Mechanical Engineering, Auburn University, Auburn, USA

<sup>b</sup> Department of Mechanical and Aerospace Engineering, University of Florida, Gainesville, USA

## ARTICLE INFO

### Article history:

Received 30 December 2020

Received in revised form 20 October 2021

Accepted 28 December 2021

Available online xxx

## ABSTRACT

Neurological conditions (NCs) can have debilitating effects on an individual and can impede a person's ability to perform activities of daily living. A common rehabilitation for individuals with NCs is the use of functional electrical stimulation (FES) to induce muscle contractions to perform a functional task, such as cycling. In this paper, we develop a closed-loop FES cycling controller that yields exponential cadence tracking. Contributions of the work result from the design and analysis innovations to compensate for switching between the different muscles and motor control inputs, compensating for the inherent uncertain nonlinear dynamics, compensating for the time-varying unknown input delay resulting from the complex electrochemical FES muscle torque production process, and compensating for saturation in the evoked torque due to fatigue, available muscle mass, or stimulation sensitivity. The performance of the developed control system was examined through a series of experiments on nine participants (five able-bodied and four with NCs). The experiments resulted in a cadence tracking error of  $-0.03 \pm 1.69$  RPM for non-informed passive able-bodied participants and  $-0.04 \pm 1.98$  RPM for the participants with NCs, for a desired cadence of 50 RPM.

© 2022 Elsevier Ltd. All rights reserved.

## 1. Introduction

Millions of individuals suffer from neurological conditions (NCs) that result in movement disorders, such as stroke, traumatic brain injury (TBI), spinal cord injuries, and Parkinson's Disease (PD), among others (Cousin, Rouse, Duenas, & Dixon, 2019). A common rehabilitative treatment for movement disorders is functional electrical stimulation (FES) to induce muscle contractions to perform functional tasks (Bellman, Downey, Parikh, & Dixon, 2017; Cousin et al., 2019; Oliveira, Costa, Pino, & Paz, 2019; Paz, Oliveira, Pino, & Fontana, 2020; Pons, Vaughan, & Jaros, 1989; Schutte, Rodgers, Zajac, & Glaser, 1993). One rehabilitative treatment for those with lower limb movement disorders is FES-cycling, which provides numerous benefits such as improved cardiovascular parameters and physiological motor control (Ferrante, Pedrocchi, Ferrigno, & Molteni, 2008; Hooker et al., 1992).

Closed-loop FES control has the potential to enable improved or new rehabilitation methods including personalized human

machine interactions. However, complications arise from inherent uncertain, nonlinear, and time-varying dynamics, switching control between multiple muscle groups and a motor (Bellman et al., 2017; Cousin et al., 2019; Downey, Merad, Gonzalez, & Dixon, 2017b), saturation of the evoked muscle torque (i.e., due to stimulation sensitivity, available muscle mass, or fatigue), and an unknown time-varying input delay between the application/removal of stimulation and the onset/end of muscle force, called the electromechanical delay (EMD)<sup>1</sup> (Allen, Stubbs, & Dixon, 2020a, 2021; Downey et al., 2017b). Furthermore, fatigue limits an exercise's duration, which can lower the exercise's rehabilitative effectiveness.

In recent years, closed-loop FES controllers have been developed to compensate for FES-induced input delays for isometric exercises (Merad, Downey, Obuz, & Dixon, 2016), leg extension exercises (Karafyllis, Malisoff, de Queiroz, Krstic, & Yang, 2015; Obuz, Duenas, Downey, Klotz, & Dixon, 2020; Sharma, Gregory, & Dixon, 2011), and for FES-cycling in the author's prior works (Allen, Cousin, Rouse, & Dixon, 2019a, 2019b, 2022; Allen, Stubbs, & Dixon, 2020b, 2020c, 2020d). For continuous exercises, such as leg extensions or isometric exercises, only the contraction delay is considered, which is the delay between the

<sup>☆</sup> The material in this paper was presented at the 3rd IFAC Workshop on Cyber-Physical & Human Systems, December 3-5, 2020, Beijing, China. This paper was recommended for publication in revised form by Associate Editor Peng Shi under the direction of Editor Thomas Parisini.

\* Corresponding author.

E-mail addresses: [bca0027@auburn.edu](mailto:bca0027@auburn.edu) (B.C. Allen), [kimberlyjstubbs@ufl.edu](mailto:kimberlyjstubbs@ufl.edu) (K.J. Stubbs), [wdixon@ufl.edu](mailto:wdixon@ufl.edu) (W.E. Dixon).

<sup>1</sup> In some literature the EMD corresponds to the time latency between the onset of EMG activity and muscle force (Nordez, Gallot, Catheline, Guével, Cornu, & Hug, 2009).

onset of stimulation and the onset of muscle force. Movements that require coordinated switching between different muscle groups, such as FES-cycling, must also consider the residual delay between the removal of stimulation and the corresponding end of muscle force production (Allen et al., 2019a, 2019b, 2022, 2020b, 2020c, 2020d). If unaccounted for, these residual forces could be produced by antagonistic muscles, which oppose the desired motion and may increase the rate of fatigue, and hence, may reduce the rehabilitative effectiveness. In Allen et al. (2019a, 2019b, 2022, 2020b), robust position and cadence tracking controllers were developed to compensate for the EMD, whereas in Allen et al. (2020c), a dual objective delayed FES cycling system was considered for both power and trajectory tracking. However, the previously developed controllers did not compensate for the saturation of the evoked muscle torques. For example, the controllers were unsaturated functions of the system's states and could produce uncomfortable or unsafe inputs if the system has large initial conditions or unmodeled disturbances. More recently, a saturated cadence tracking controller was developed in Allen et al. (2020d) to compensate for the EMD; however, the developed control system resulted in a relatively large steady-state cadence tracking error.

Non-FES related systems with input delays have extensively been studied (cf., Bagheri, Naseradinmousavi, & Krstic, 2019; Fischer, Dani, Sharma, & Dixon, 2013a; Karafyllis & Krstic, 2017; Krstic, 2009, 2010; Mazenc & Malisoff, 2020; Mazenc, Malisoff, & Ozbay, 2018; Mazenc, Mondie, Francisco, Conge, Lorraine, & Metz, 2004; Wang, Niu, Wu, & Xie, 2018; Wang, Sun, & Mazenc, 2016; Yang, Li, & Qiu, 2019; Zhou & Lin, 2011; Zhou, Lin, & Duan, 2010; Zhou, Wu, & Shi, 2017), but few studies have considered systems with switched dynamics (Mazenc et al., 2018; Wang et al., 2018, 2016; Yang et al., 2019) and few have implemented saturated control (Fischer et al., 2013a; Krstic, 2010; Mazenc et al., 2004; Zhou & Lin, 2011; Zhou et al., 2010, 2017). Most saturated controllers for input delayed systems have been for linear systems (Zhou & Lin, 2011; Zhou et al., 2010), with a few exceptions that include nonlinear systems (Fischer et al., 2013a; Krstic, 2010; Mazenc et al., 2004; Zhou et al., 2017). Strict-feedforward nonlinear systems are considered with no disturbances in Mazenc et al. (2004) and with no uncertainties in Krstic (2010). A class of uncertain nonlinear systems are considered in Fischer et al. (2013a) with known and constant input delays and in Zhou et al. (2017) with unknown delays. However, the aforementioned results either are not for switched systems or do not implement a saturated controller. Furthermore, non-FES related systems do not compensate for FES specific factors, such as the need to properly time stimulation to yield effective agonist muscle contractions and to remove/limit residual antagonistic forces.

Building on our precursory result in Allen et al. (2020d), this paper modifies the control development and Lyapunov-based stability analysis to compensate for the EMD and to ensure both exponential position and cadence tracking of a switched FES-cycle system using saturated FES control. Furthermore, compared to Allen et al. (2020d), this work improves the gain conditions and provides comparative experiments on four and five participants with and without NCs, respectively. The controllers developed in this work are robust to unknown disturbances, uncertainties in the dynamics, and the unknown time-varying EMD. To properly schedule the application of the FES, switching signals and trigger conditions were developed that are state and delay dependent, which ensure muscle contractions occur in efficient regions of the crank cycle. An important feature of the bound on the developed saturated FES controller is that it is known a priori and can be adjusted by tuning the control gains to limit the stimulation levels, providing a more comfortable experience for the participant.

Comparative experiments were performed on five able-bodied participants using both the controllers developed in this work and the control system developed in Allen et al. (2020d) to demonstrate the performance of each method. The results indicate that the controller developed in this work significantly improved the cadence tracking while simultaneously reducing the required control effort. Furthermore, active therapy (i.e., the participant provided volitional effort) experiments were performed on four participants with NCs (e.g., cerebral palsy, spina bifida, and multiple sclerosis), which further validated the performance of the developed control system.

## 2. Dynamics

Throughout this work, delayed functions are denoted as

$$f_\tau \triangleq \begin{cases} f(t - \tau(t)), & t - \tau(t) \geq t_0 \\ 0, & t - \tau(t) < t_0 \end{cases},$$

where  $t \in \mathbb{R}_{\geq 0}$ ,  $t_0 \in \mathbb{R}_{\geq 0}$ ,  $\tau : \mathbb{R}_{\geq 0} \rightarrow \mathbb{S}$ , and  $\mathbb{S} \subset \mathbb{R}_{>0}$  denote the time, initial time, the EMD, and the set of potential delay values (Allen et al., 2020a, 2021), respectively. The combined cycle-rider dynamics are modeled as (Bellman et al., 2017)<sup>2</sup>

$$M(q)\ddot{q} + V(q, \dot{q})\dot{q} + G(q) + P(q, \dot{q}) + b_c\dot{q} + d(t) = \tau_{vol}(t) + B_E u_e(t) + B_M^c(q, \dot{q}, \tau, t) u_\tau, \quad (1)$$

where  $q : \mathbb{R}_{\geq 0} \rightarrow \mathcal{Q}$ ,  $\dot{q} : \mathbb{R}_{\geq 0} \rightarrow \mathbb{R}$ ,  $\ddot{q} : \mathbb{R}_{\geq 0} \rightarrow \mathbb{R}$ , and  $\mathcal{Q} \subseteq \mathbb{R}$  denote the measurable crank angle, measurable crank velocity (cadence), unmeasurable crank acceleration, and the set of potential crank angles, respectively. Furthermore,  $M : \mathcal{Q} \rightarrow \mathbb{R}_{>0}$ ,  $V : \mathcal{Q} \times \mathbb{R} \rightarrow \mathbb{R}$ ,  $G : \mathcal{Q} \rightarrow \mathbb{R}$ ,  $P : \mathcal{Q} \times \mathbb{R} \rightarrow \mathbb{R}$ ,  $b_c \in \mathbb{R}_{>0}$ , and  $d : \mathbb{R}_{\geq 0} \rightarrow \mathbb{R}$  denote the inertial, centripetal-Coriolis, gravitational, passive viscoelastic tissue, viscous damping, and disturbance effects, respectively. The torque about the crank produced by volitional effort is denoted as  $\tau_{vol} : \mathbb{R}_{\geq 0} \rightarrow \mathbb{R}$ . Let  $B_E \in \mathbb{R}_{>0}$ ,  $u_e : \mathbb{R}_{\geq 0} \rightarrow \mathbb{R}$ ,  $B_M^c : \mathcal{Q} \times \mathbb{R} \times \mathbb{S} \times \mathbb{R}_{\geq 0} \rightarrow \mathbb{R}_{\geq 0}$ ,  $u_\tau : \mathbb{S} \times \mathbb{R}_{\geq 0} \rightarrow \mathbb{R}$ , and  $u : \mathbb{R}_{\geq 0} \rightarrow \mathbb{R}$  denote the unknown motor control effectiveness, motor control input, unknown FES control effectiveness, delayed FES control input, and the implemented FES control input that is subsequently designed. The motor control effectiveness is defined as  $B_E \triangleq B_e k_e$ , where  $k_e, B_e \in \mathbb{R}_{>0}$  denote a selectable constant and the unknown motor effectiveness, respectively. Likewise, define the FES control effectiveness as

$$B_M^c(q, \dot{q}, \tau, t) \triangleq \sum_{m \in \mathcal{M}} B_m(q, \dot{q}, t) k_m \sigma_{m, \tau}, \quad (2)$$

where for each muscle group (i.e.,  $\forall m \in \mathcal{M}$ ),  $B_m : \mathcal{Q} \times \mathbb{R} \times \mathbb{R}_{\geq 0} \rightarrow \mathbb{R}_{>0}$ ,  $k_m \in \mathbb{R}_{>0}$ , and  $\sigma_{m, \tau}$  denote the unknown muscle effectiveness, a selectable constant, and a delayed FES switching signal, respectively. The set  $\mathcal{M} \triangleq \{LH, LQ, LG, RH, RQ, RG\}$  denotes the left (L) and right (R) hamstrings (H), quadriceps femoris (Q), and gluteal (G) muscle groups. Notice that the delayed FES switching signals,  $\sigma_{m, \tau}$ ,  $\forall m \in \mathcal{M}$ , indicate the muscle groups that were stimulated at time  $t - \tau$  by the delayed FES control input,  $u_\tau$ .

The implemented FES switching signals, denoted as  $\sigma_m : \mathcal{Q} \times \mathbb{R} \rightarrow \{0, 1\}$ ,  $\forall m \in \mathcal{M}$ , are piecewise right-continuous and designed as

$$\sigma_m(q, \dot{q}) \triangleq \begin{cases} 1, & q_\alpha(q, \dot{q}) \in \mathcal{Q}_m, \forall m \in \mathcal{M}, \\ 0, & \text{otherwise} \end{cases}, \quad (3)$$

where  $q_\alpha : \mathcal{Q} \times \mathbb{R} \rightarrow \mathbb{R}$  is a trigger condition, which considers bounds on the EMD (e.g., see Merad et al., 2016) to effectively project the crank position,  $q$ , forward to determine when to stimulate each muscle group to induce kinematically efficient

<sup>2</sup> For notational brevity, all explicit dependence on time,  $t$ , within the terms  $q(t)$ ,  $\dot{q}(t)$ ,  $\ddot{q}(t)$  is suppressed.

muscle contractions. The set of angles, denoted by  $\mathcal{Q}_m \subset \mathcal{Q}$ ,  $\forall m \in \mathcal{M}$ , where a contraction of muscle  $m$  is kinematically efficient to contribute to forward pedaling (i.e., positive crank motion) is defined as in Bellman et al. (2017) as

$$\mathcal{Q}_m \triangleq \{q \in \mathcal{Q} \mid T_m(q) > \varepsilon_m\}, \forall m \in \mathcal{M}, \quad (4)$$

where  $T_m : \mathcal{Q} \rightarrow \mathbb{R}$  and  $\varepsilon_m \in \mathbb{R}_{>0}$  denote a torque transfer ratio and a lower threshold, respectively. Define the desired contraction regions of the cycle as  $\mathcal{Q}_{FES} \triangleq \bigcup_{m \in \mathcal{M}} \{\mathcal{Q}_m\}$  and the inefficient regions (i.e., kinematic deadzones) as  $\mathcal{Q}_{KDZ} \triangleq \mathcal{Q} \setminus \mathcal{Q}_{FES}$ .

The exact values of the parameters in (1) are unknown for the cycle-rider system; however, the subsequent analysis only requires bounds for the aforementioned parameters (cf., Bellman et al., 2017). **Property: 1** The inertial, centripetal-Coriolis, gravitational, passive viscoelastic tissue, viscous damping, disturbance, and volitional contribution terms can be bounded as  $c_m \leq M \leq c_M$ ,  $|V| \leq c_V |\dot{q}|$ ,  $|G| \leq c_G$ ,  $|P| \leq c_{P_1} + c_{P_2} |\dot{q}|$ ,  $b_c \dot{q} \leq c_c |\dot{q}|$ ,  $|d| \leq c_d$ , and  $|\tau_{vol}| \leq c_{vol}$ , respectively, where  $c_m, c_M, c_V, c_G, c_{P_1}, c_{P_2}, c_c, c_d, c_{vol} \in \mathbb{R}_{>0}$  are known constants (Bellman et al., 2017). **Property: 2** The FES and motor control effectiveness terms can be bounded as  $c_b \leq B_M^r \leq c_B$  (when  $\sum_{m \in \mathcal{M}} \sigma_{m,\tau} > 0$ ) and  $c_e \leq B_E \leq c_E$ , respectively, where  $c_b, c_B, c_e, c_E \in \mathbb{R}_{>0}$  are known constants (Bellman et al., 2017). **Property: 3** The EMD is bounded as  $\underline{\tau} \leq \tau \leq \bar{\tau}$ , where  $\underline{\tau}, \bar{\tau} \in \mathbb{R}_{>0}$  are known constants (Allen et al., 2020a, 2021).

### 3. Control development

#### 3.1. Error system

The first control objective of the FES-cycle system is for the crank to track a sufficiently smooth desired position  $q_d : \mathbb{R}_{\geq 0} \rightarrow \mathbb{R}$  and desired cadence  $\dot{q}_d : \mathbb{R}_{\geq 0} \rightarrow \mathbb{R}$ , which is complicated by the existence of uncertainties in the dynamic model and the unknown time-varying EMD. The tracking control objective is quantified by a measurable position tracking error, denoted by  $e : \mathbb{R}_{\geq 0} \rightarrow \mathbb{R}$ , and defined as<sup>3</sup>

$$e \triangleq q_d - q, \quad (5)$$

and a measurable cadence tracking error, denoted by  $\dot{e} : \mathbb{R}_{\geq 0} \rightarrow \mathbb{R}$ , and defined as

$$\dot{e} \triangleq \dot{q}_d - \dot{q}. \quad (6)$$

Motivated by the desire to inject a delay-free FES input into the open- and closed-loop error systems, an auxiliary signal  $e_u : \mathbb{R}_{\geq 0} \rightarrow \mathbb{R}$  is designed as

$$e_u \triangleq - \int_{t-\hat{\tau}}^t \sigma_s(\theta) u(\theta) d\theta, \quad (7)$$

where  $\hat{\tau} \in \mathbb{R}_{>0}$  denotes a constant estimate of the EMD, and  $\sigma_s : \mathbb{R}_{\geq 0} \rightarrow \{0, 1\}$  is a piecewise right-continuous switching signal that indicates when stimulation is applied and is defined as

$$\sigma_s(t) \triangleq \begin{cases} 1, & \sum_{m \in \mathcal{M}} \sigma_m > 0 \\ 0, & \text{otherwise} \end{cases}. \quad (8)$$

The EMD estimation error is defined as  $\tilde{\tau} \triangleq \tau - \hat{\tau}$ , which can be upper bounded by applying Property 3 as  $|\tilde{\tau}| \leq \bar{\tau}$ , where  $\bar{\tau} \in \mathbb{R}_{>0}$  is a known constant.

The second control objective of the FES-cycle system is to design a saturated FES control input to ensure the comfort of the

participant. The FES input can be bounded a priori by embedding the FES input in a bounded and smooth trigonometric term, such as  $\tanh(\cdot)$ ; however, complications arise in the stability analysis due to the existence of the EMD as seen in Allen et al. (2020d). Motivated to enable the subsequent stability analysis and to include  $e$  in the closed-loop error system, a measurable auxiliary tracking error,  $r : \mathbb{R}_{\geq 0} \rightarrow \mathbb{R}$ , is defined as

$$r \triangleq \dot{e} + \alpha_1 e + \tanh(e_f) + \alpha_2 e_u, \quad (9)$$

where  $\alpha_1, \alpha_2 \in \mathbb{R}_{>0}$  are selectable constants, and  $e_f : \mathbb{R}_{\geq 0} \rightarrow \mathbb{R}$  is the solution to

$$\dot{e}_f \triangleq \cosh^2(e_f) (-k_1 r + e - \alpha_3 \tanh(e_f)), \quad (10)$$

where hyperbolic functions are used to facilitate the saturated control design,  $e_f(0) = 0$ , and  $k_1, \alpha_3 \in \mathbb{R}_{>0}$  are selectable constants.

#### 3.2. Open-loop error system

To obtain the open-loop error system, we substitute (6) into (9) and take the time derivative of (9), apply Leibniz integral rule to (7) to obtain  $\dot{e}_u$ , solve (1) for  $\ddot{q}$ , substitute in (10), and add and subtract  $B_M^r M^{-1} u_{\hat{\tau}} + e$  to yield

$$\begin{aligned} \dot{r} = & \chi + \frac{B_M^r}{M} (u_{\hat{\tau}} - u_{\tau}) - \frac{B_E}{M} u_e - k_1 r \\ & - \sigma_s \alpha_2 u + \left( \sigma_{s,\hat{\tau}} \alpha_2 - \frac{B_M^r}{M} \right) u_{\hat{\tau}} - e, \end{aligned} \quad (11)$$

where  $\chi : \mathcal{Q} \times \mathbb{R} \times \mathbb{R} \times \mathbb{R} \times \mathbb{R}_{\geq 0} \rightarrow \mathbb{R}$  is defined as

$$\begin{aligned} \chi \triangleq & \ddot{q}_d + M^{-1} [V\dot{q} + G + P + b_c \dot{q} + d - \tau_{vol}] \\ & + 2e + \alpha_1 \dot{e} - \alpha_3 \tanh(e_f). \end{aligned} \quad (12)$$

By using (6), (9), and Property 1,

$$|\chi| \leq \Phi + \rho(\|z\|) \|z\|, \quad (13)$$

where  $\Phi \in \mathbb{R}_{>0}$  is a known constant,  $\rho(\cdot)$  is a globally invertible, positive, radially unbounded, and strictly increasing function, and  $z \in \mathbb{R}^4$  is a composite error vector defined as

$$z \triangleq \begin{bmatrix} e & r & e_u & \tanh(e_f) \end{bmatrix}^T. \quad (14)$$

#### 3.3. Closed-loop error system

The FES and motor control inputs are designed, based on (11) and the subsequent stability analysis, as

$$u \triangleq - \frac{k_1}{\alpha_2} \tanh(e_f), \quad (15)$$

$$u_e \triangleq \frac{c_M}{c_e} (\sigma_e k_2 r + k_3 \text{sgn}(r)), \quad (16)$$

where  $\text{sgn}(\cdot)$  denotes the signum function, and  $k_1, k_2, k_3 \in \mathbb{R}_{>0}$  are selectable constants. The motor switching signal, denoted by  $\sigma_e : \mathcal{Q} \times \{0, 1\} \rightarrow \{0, 1\}$ , is piecewise right-continuous and defined as

$$\sigma_e(q, \sigma_s) \triangleq \begin{cases} 1, & q \in \mathcal{Q}_{KDZ} \\ 1, & q \in \mathcal{Q}_{FES}, \sigma_s = 0 \\ 0, & \text{otherwise} \end{cases}. \quad (17)$$

Notice that  $\sigma_e$  is designed to activate the  $k_2 r$  motor term whenever muscle forces are small (i.e.,  $q \in \mathcal{Q}_{KDZ}$ ) or whenever muscle contractions are present but stimulation is not actively being applied ( $q \in \mathcal{Q}_{FES}, \sigma_s = 0$ ).

A feature of the FES control input is that  $|u| \leq \frac{k_1}{\alpha_2}$ , and thus it can be bounded by selectable gain constants. The stimulation input (i.e. pulse width) to each muscle group is defined as  $u_m \triangleq k_m \sigma_m u$ ,  $\forall m \in \mathcal{M}$ , resulting in a bounded stimulation input since  $|u_m| \leq \frac{k_m k_1}{\alpha_2}$ ,  $\forall m \in \mathcal{M}$ . Therefore, the stimulation input into each

<sup>3</sup> For notational brevity, all functional dependencies are hereafter suppressed unless required for clarity of exposition.

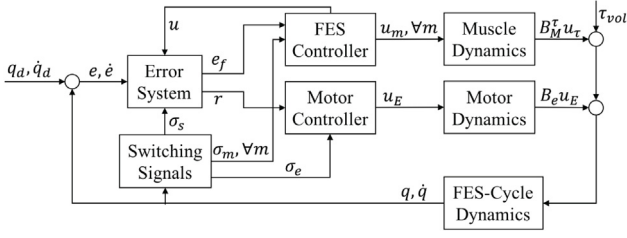


Fig. 1. Block diagram representing the closed-loop feedback structure of the cycle-rider system.

muscle can be bounded a priori by selectable constants to ensure a more comfortable and safer experience for the rider. The motor control input is defined as  $u_E \triangleq k_e u_e$ . The closed-loop error system is obtained by substituting (15) and (16) into (11) to yield

$$\begin{aligned} \dot{r} = & \chi + \frac{B_M^T}{M} (u_{\hat{\tau}} - u_{\tau}) - k_1 r - e \\ & - \frac{B_E}{M} \frac{c_M}{c_e} (\sigma_e k_2 r + k_3 \text{sgn}(r)) \\ & + \sigma_s k_1 \tanh(e_f) + (\sigma_{s,\hat{\tau}} \alpha_2 - \frac{B_M^T}{M}) u_{\hat{\tau}}. \end{aligned} \quad (18)$$

A block diagram of the closed-loop control structure is shown in Fig. 1.

### 3.4. Gain conditions and auxiliary terms

To facilitate the subsequent stability analysis, auxiliary terms  $Q_1, Q_2 : \mathbb{R}_{\geq 0} \rightarrow \mathbb{R}_{\geq 0}$  are defined as

$$Q_1 \triangleq \frac{1}{2} (\varepsilon_1 \omega_1 + \omega_2) \int_{t-\hat{\tau}}^t u^2(\theta) d\theta, \quad (19)$$

$$Q_2 \triangleq \frac{\omega_3}{\hat{\tau}} \int_{t-\hat{\tau}}^t \int_s^t u^2(\theta) d\theta ds, \quad (20)$$

and auxiliary bounding constants  $\beta_1, \beta_2, \delta_1, \delta_2 \in \mathbb{R}$  are defined as

$$\begin{aligned} \beta_1 \triangleq & \min \left( \alpha_1 - \frac{\alpha_2 \varepsilon_2}{2}, \frac{1}{2} (k_1 - \omega_2), \frac{\omega_3}{3\hat{\tau}^2} - \frac{\alpha_2}{2\varepsilon_2} \right. \\ & \left. - \frac{\omega_1}{\varepsilon_1}, \alpha_3 - \frac{k_1^2}{\alpha_2^2} (\varepsilon_1 \omega_1 + \frac{1}{2} \omega_2 + \omega_3) \right), \end{aligned} \quad (21)$$

$$\begin{aligned} \beta_2 \triangleq & \min \left( \alpha_1 - \frac{\alpha_2 \varepsilon_2}{2}, k_2 - \frac{1}{2} \omega_2, \frac{\omega_3}{3\hat{\tau}^2} - \frac{\alpha_2}{2\varepsilon_2} \right. \\ & \left. - \frac{\omega_1}{\varepsilon_1}, \alpha_3 - \frac{k_1}{2} - \frac{k_1^2}{\alpha_2^2} (\varepsilon_1 \omega_1 + \frac{1}{2} \omega_2 + \omega_3) \right), \end{aligned} \quad (22)$$

$$\delta_1 \triangleq \min \left( \frac{1}{2} \beta_1, \frac{\omega_3}{3\hat{\tau} (\frac{1}{2} (\varepsilon_1 \omega_1 + \omega_2))}, \frac{1}{3\hat{\tau}} \right), \quad (23)$$

$$\delta_2 \triangleq \min \left( \frac{1}{2} \beta_2, \frac{\omega_3}{3\hat{\tau} (\frac{1}{2} (\varepsilon_1 \omega_1 + \omega_2))}, \frac{1}{3\hat{\tau}} \right), \quad (24)$$

where  $\varepsilon_1, \varepsilon_2, \omega_1, \omega_2, \omega_3 \in \mathbb{R}_{>0}$  are selectable constants. To ensure that (21)–(24) are positive, the following gain conditions must be satisfied

$$\alpha_1 > \frac{1}{2} \alpha_2 \varepsilon_2, \quad k_1 > \omega_2, \quad k_2 > \frac{1}{2} \omega_2, \quad (25)$$

$$k_3 \geq \Phi + \bar{\tau} \gamma \frac{c_B}{c_M} + \frac{k_1}{\alpha_2} \max \left( \frac{c_B}{c_M}, \alpha_2 \right), \quad (26)$$

$$\omega_2 \geq \max \left( \left| \alpha_2 - \frac{c_B}{c_M} \right|, \left| \alpha_2 - \frac{c_B}{c_M} \right| \right), \quad (27)$$

$$\omega_3 > 3\hat{\tau}^2 \left( \frac{\alpha_2}{2\varepsilon_2} + \frac{\omega_1}{\varepsilon_1} \right), \quad (28)$$

$$\alpha_3 > \frac{1}{2} k_1 + \frac{k_1^2}{\alpha_2^2} \left( \varepsilon_1 \omega_1 + \frac{1}{2} \omega_2 + \omega_3 \right), \quad (29)$$

where  $\gamma \in \mathbb{R}_{>0}$  is a known constant.

## 4. Stability analysis

Switching times are denoted by  $\{t_n^i\}$ ,  $i \in \{m, e\}$ ,  $n \in \{0, 1, 2, \dots\}$ , which represent the instants in time when  $\sigma_e$  becomes zero ( $i = m$ ) or nonzero ( $i = e$ ). A common Lyapunov function candidate,  $V_L : \mathcal{D} \rightarrow \mathbb{R}_{\geq 0}$ , that is continuously differentiable and positive definite is defined on a domain  $\mathcal{D} \subseteq \mathbb{R}^6$  as

$$V_L(y) \triangleq \frac{1}{2} e^2 + \frac{1}{2} r^2 + \frac{1}{2} \omega_1 e_u^2 + \frac{1}{2} \tanh^2(e_f) + Q_1 + Q_2, \quad (30)$$

where  $y \in \mathbb{R}^6$  is defined as

$$y \triangleq \left[ z^T \quad \sqrt{Q_1} \quad \sqrt{Q_2} \right]^T. \quad (31)$$

The common Lyapunov function candidate in (30) can be bounded as

$$\lambda_1 \|y\|^2 \leq V_L \leq \lambda_2 \|y\|^2, \quad (32)$$

where  $\lambda_1, \lambda_2 \in \mathbb{R}_{>0}$  are known constants defined as

$$\lambda_1 \triangleq \min \left( \frac{1}{2}, \frac{\omega_1}{2} \right), \quad \lambda_2 \triangleq \max \left( 1, \frac{\omega_1}{2} \right).$$

Let  $S_{\mathcal{D}}$  be defined as

$$S_{\mathcal{D}} \triangleq \left\{ y \in \mathcal{D} \mid \|y\| < \sqrt{\frac{\lambda_1}{\lambda_2}} \gamma \right\}, \quad (33)$$

where  $\gamma \in \mathbb{R}_{>0}$  is a known constant defined as<sup>4</sup>  $\gamma \triangleq \inf \left\{ \rho^{-1} \left( \left( \sqrt{\frac{1}{2} k_1 \min(\beta_1, \beta_2)}, \infty \right) \right) \right\}$ .

**Theorem 1.** For the motorized FES cycle-rider dynamics in (1) and Properties 1–3, the controllers defined in (15) and (16) yield exponential cadence tracking in the sense that

$$\|y(t)\| \leq \sqrt{\frac{\lambda_2}{\lambda_1}} \|y(t_0)\| \exp \left( -\frac{\lambda_3}{2} (t - t_0) \right), \quad (34)$$

$\forall t \in [t_0, \infty)$ , where  $\lambda_3 \triangleq \lambda_2^{-1} \min(\delta_1, \delta_2)$ , provided  $y(t_0) \in S_{\mathcal{D}}$ , and the gain conditions in (25)–(29) are satisfied.

**Proof.** Since the FES and motor controllers are discontinuous, a generalized solution exists almost everywhere (a.e.) within  $t \in [t_0, \infty)$  for the time derivative of (30), denoted by  $\dot{V}_L$ , such that  $\dot{V}_L(y) \stackrel{\text{a.e.}}{=} \dot{V}_L(y)$ . Let  $y(t)$  be a Filippov solution to the differential inclusion  $\dot{y} \in K[h](y)$  for  $t \in [t_0, \infty)$ , where  $K[\cdot]$  is defined as in Filippov (1964), and let  $h : \mathbb{R}^6 \rightarrow \mathbb{R}^6$  be defined as  $h \triangleq \left[ \dot{e} \quad \dot{r} \quad \dot{e}_u \quad \tanh(e_f) \quad \sqrt{Q_1} \quad \sqrt{Q_2} \right]^T$  (see Fischer, Kamalapurkar, & Dixon, 2013b). Using the calculus of  $K[\cdot]$  from Paden and Sastry (1987), using (10), (9), and (18), applying the Leibniz integral rule to (7), (19), (20), and canceling common terms yield the following generalized time derivative of (30),

$$\begin{aligned} \dot{V}_L \subseteq & e(-\alpha_1 e - \alpha_2 e_u) + r \left[ \frac{K[B_M^T]}{M} (u_{\hat{\tau}} - u_{\tau}) \right. \\ & \left. - \frac{B_E}{M} \frac{c_M}{c_e} (K[\sigma_e] k_2 r + k_3 K[\text{sgn}(r)]) \right. \\ & \left. + \chi - k_1 r + K[\sigma_s] k_1 \tanh(e_f) \right. \\ & \left. + \left( K[\sigma_{s,\hat{\tau}}] \alpha_2 - \frac{K[B_M^T]}{M} \right) u_{\hat{\tau}} \right] \\ & + \omega_1 e_u (-K[\sigma_s] u + K[\sigma_{s,\hat{\tau}}] u_{\hat{\tau}}) \\ & + \tanh(e_f) (-k_1 r - \alpha_3 \tanh(e_f)) \\ & + \frac{1}{2} (\varepsilon_1 \omega_1 + \omega_2) (u^2 - u_{\hat{\tau}}^2) \\ & + \frac{\omega_3}{\hat{\tau}} \left( \hat{\tau} u^2 - \int_{t-\hat{\tau}}^t u^2(\theta) d\theta \right), \end{aligned} \quad (35)$$

<sup>4</sup> For a set  $A$ , the inverse image is defined as  $\rho^{-1}(A) \triangleq \{a \mid \rho(a) \in A\}$ .

**Table 1**  
Summary of all potential switching cases.

Case number	$\sigma_s$	$\sigma_{s,\hat{\tau}}$	$\sigma_{s,\tau}^a$	$\sigma_e$
1	1	1	1	0
2	1	1	1	1
3	1	1	0	1
4	1	0	1	1
5	1	0	0	1
6	0	1	1	1
7	0	0	1	1
8	0	1	0	1
9	0	0	0	1

<sup>a</sup>From (2), (8), and Property 2,  $B_M^r = 0$  if and only if  $\sigma_{s,\tau} = 0$ .

where,  $K[\text{sgn}(\cdot)] = \text{SGN}(\cdot)$  such that  $\text{SGN}(\cdot) = \{1\}$  if  $(\cdot) > 0$ ,  $[-1, 1]$  if  $(\cdot) = 0$ , and  $\{-1\}$  if  $(\cdot) < 0$ . Evaluating the expression in (35) for each potential combination of the switching signals will yield a result for all time. By inspection of (35) and the switching conditions in (3), (17), and (8), there exist nine unique combinations as summarized in Table 1. Subsequently, Case 1 will be considered, followed by an examination of Cases 2-9 using an overall upper bound.

From Table 1, Case 1 represents the only case when  $\sigma_e = 0$  (i.e.,  $t \in [t_n^m, t_{n+1}^e)$ ), which occurs when FES forces are occurring. Notice that the switching signals are constant during a given case; thus, during Case 1,  $K[\sigma_s] = 1$ ,  $K[\sigma_{s,\hat{\tau}}] = 1$ ,  $K[\sigma_e] = 0$ , and by Property 2,  $c_b \leq K[B_M^r] \leq c_B$ . Setting  $K[\sigma_s] = 1$ ,  $K[\sigma_{s,\hat{\tau}}] = 1$ , and  $K[\sigma_e] = 0$ , choosing  $\omega_2$  such that  $\max\left(\left|\alpha_2 - \frac{c_b}{c_M}\right|, \left|\alpha_2 - \frac{c_B}{c_M}\right|\right) \leq \omega_2$ , using the fact that  $\dot{V}_L(y) \stackrel{\text{a.e.}}{\leq} \dot{\hat{V}}_L(y)$ , and using Properties 1 and 2 yields the following upper bound for (35) during Case 1,

$$\begin{aligned} \dot{V}_L \stackrel{\text{a.e.}}{\leq} & -\alpha_1 e^2 + \alpha_2 |ee_u| + \frac{c_B}{c_M} |r| |u_{\hat{\tau}} - u_{\tau}| \\ & + |r| |\chi| - k_3 |r| - k_1 r^2 + \omega_2 |u_{\hat{\tau}} r| \\ & + \omega_1 |e_u u| + \omega_1 |e_u u_{\hat{\tau}}| - \alpha_3 \tanh^2(e_f) \\ & + \frac{1}{2} (\varepsilon_1 \omega_1 + \omega_2) (u^2 - u_{\hat{\tau}}^2) \\ & + \frac{\omega_3}{\hat{\tau}} \left( \hat{\tau} u^2 - \int_{t-\hat{\tau}}^t u^2(\theta) d\theta \right). \end{aligned} \tag{36}$$

Using (10), (15), and (31) it could be shown that  $\dot{u}(\cdot) \leq \mathcal{Y}, \forall \cdot \in [t_0, t)$  provided that  $\|y(\cdot)\| < \gamma, \forall \cdot \in [t_0, t)$ . Since  $\dot{u}(\cdot) \leq \mathcal{Y}, \forall \cdot \in [t_0, t)$ , the Mean Value Theorem can be applied to upper bound (36) as

$$\begin{aligned} \dot{V}_L \stackrel{\text{a.e.}}{\leq} & -\alpha_1 e^2 + \alpha_2 |ee_u| + \bar{\tau} \mathcal{Y} \frac{c_B}{c_M} |r| + |r| |\chi| \\ & - k_3 |r| - k_1 r^2 + \omega_2 |u_{\hat{\tau}} r| + \omega_1 |e_u u| \\ & + \omega_1 |e_u u_{\hat{\tau}}| - \alpha_3 \tanh^2(e_f) \\ & + \frac{1}{2} (\varepsilon_1 \omega_1 + \omega_2) (u^2 - u_{\hat{\tau}}^2) \\ & + \frac{\omega_3}{\hat{\tau}} \left( \hat{\tau} u^2 - \int_{t-\hat{\tau}}^t u^2(\theta) d\theta \right). \end{aligned} \tag{37}$$

Substituting (13) into (37), applying the gain condition in (26), and completing the squares on the  $|r| \rho(\|z\|) \|z\|$  term yields

$$\begin{aligned} \dot{V}_L \stackrel{\text{a.e.}}{\leq} & -\alpha_1 e^2 + \alpha_2 |ee_u| - \frac{1}{2} k_1 r^2 + \omega_2 |u_{\hat{\tau}} r| \\ & + \omega_1 |e_u u| + \omega_1 |e_u u_{\hat{\tau}}| - \alpha_3 \tanh^2(e_f) \\ & + \frac{1}{2} (\varepsilon_1 \omega_1 + \omega_2) (u^2 - u_{\hat{\tau}}^2) + \omega_3 u^2 \\ & - \frac{\omega_3}{\hat{\tau}} \int_{t-\hat{\tau}}^t u^2(\theta) d\theta + \frac{1}{2k_1} \rho^2(\|z\|) \|z\|^2. \end{aligned} \tag{38}$$

Applying Young's Inequality and using (15) yields

$$\begin{aligned} \dot{V}_L \stackrel{\text{a.e.}}{\leq} & -\left(\alpha_1 - \frac{\omega_2 \varepsilon_2}{2}\right) e^2 + \left(\frac{\alpha_2}{2\varepsilon_2} + \frac{\omega_1}{\varepsilon_1}\right) e_u^2 \\ & - \frac{1}{2} (k_1 - \omega_2) r^2 - \alpha_3 \tanh^2(e_f) \\ & + \frac{k_1^2}{\alpha_2} (\varepsilon_1 \omega_1 + \frac{1}{2} \omega_2 + \omega_3) \tanh^2(e_f) \\ & - \frac{\omega_3}{\hat{\tau}} \int_{t-\hat{\tau}}^t u^2(\theta) d\theta + \frac{1}{2k_1} \rho^2(\|z\|) \|z\|^2. \end{aligned} \tag{39}$$

We can bound  $Q_2$  as

$$Q_2 \leq \omega_3 \int_{t-\hat{\tau}}^t u^2(\theta) d\theta, \tag{40}$$

and then apply the Cauchy-Schwarz inequality to (7) to obtain

$$e_u^2 \leq \hat{\tau} \int_{t-\hat{\tau}}^t u^2(\theta) d\theta. \tag{41}$$

From (19), (40), and (41),

$$\begin{aligned} -\frac{\omega_3}{\hat{\tau}} \int_{t-\hat{\tau}}^t u^2(\theta) d\theta & \leq -\frac{\omega_3}{3\hat{\tau}(\frac{1}{2}(\varepsilon_1 \omega_1 + \omega_2))} Q_1 \\ & - \frac{\omega_3}{3\hat{\tau}^2} e_u^2 - \frac{1}{3\hat{\tau}} Q_2. \end{aligned} \tag{42}$$

Substituting (42) into (39), using the fact that  $\|y\| \geq \|z\|$ , and using (14), (21), (23), and (32) yields

$$\dot{V}_L \stackrel{\text{a.e.}}{\leq} -\frac{\delta_1}{\lambda_2} V_L, \tag{43}$$

$\forall t \in [t_n^m, t_{n+1}^e)$ , provided that  $\|y(\cdot)\| < \gamma, \forall \cdot \in [t_0, t)$  and provided  $y(t_n^m) \in \mathcal{D}$ , where

$$\mathcal{D} \triangleq \{y \in \mathbb{R}^6 \mid \|y\| < \gamma\}. \tag{44}$$

The condition  $y(t_n^m) \in \mathcal{D}$  is equivalent to requiring  $\|y(t_n^m)\| < \gamma$ .

Cases 2-9 from Table 1 all include  $\sigma_e = 1$  (i.e.,  $t \in [t_n^e, t_{n+1}^m)$ ). To facilitate the development of an overall upper bound for Cases 2-9, notice that by considering each case individually, selecting  $\omega_2$  according to (27), and using Properties 1 and 2, it could be shown that

$$\left| \left( K[\sigma_{s,\hat{\tau}}] \alpha_2 - \frac{K[B_M^r]}{M} \right) \right| \leq \omega_2 + \max\left(\frac{c_b}{c_M}, \alpha_2\right). \tag{45}$$

An overall upper bound of (35) for Cases 2-9 is obtained by considering each case individually, using Properties 1 and 2, and using (45) to yield

$$\begin{aligned} \dot{V}_L \stackrel{\text{a.e.}}{\leq} & -\alpha_1 e^2 + \alpha_2 |ee_u| + |r| |\chi| - k_3 |r| - k_1 r^2 \\ & + \frac{c_B}{c_M} |r| |u_{\hat{\tau}} - u_{\tau}| - k_2 r^2 + \omega_2 |u_{\hat{\tau}} r| \\ & + \max\left(\frac{c_b}{c_M}, \alpha_2\right) |u_{\hat{\tau}} r| - \alpha_3 \tanh^2(e_f) \\ & + \omega_1 |e_u u| + \omega_1 |e_u u_{\hat{\tau}}| + k_1 |r \tanh(e_f)| \\ & + \frac{1}{2} (\varepsilon_1 \omega_1 + \omega_2) (u^2 - u_{\hat{\tau}}^2) \\ & + \frac{\omega_3}{\hat{\tau}} \left( \hat{\tau} u^2 - \int_{t-\hat{\tau}}^t u^2(\theta) d\theta \right). \end{aligned} \tag{46}$$

Substituting (13) into (46), completing the squares on  $|r| \rho(\|z\|) \|z\|$ , using Young's Inequality on  $|r \tanh(e_f)|$ , and using the fact that  $|u_{\hat{\tau}} r| \leq \frac{k_1}{\alpha_2} |r|$  yields

$$\begin{aligned} \dot{V}_L \stackrel{\text{a.e.}}{\leq} & -\alpha_1 e^2 + \alpha_2 |ee_u| + |r| \Phi - k_3 |r| - k_2 r^2 \\ & + \frac{1}{2k_1} \rho^2(\|z\|) \|z\|^2 + \frac{c_B}{c_M} |r| |u_{\hat{\tau}} - u_{\tau}| \\ & + \omega_2 |u_{\hat{\tau}} r| + \frac{k_1}{\alpha_2} \max\left(\frac{c_b}{c_M}, \alpha_2\right) |r| \\ & + \omega_1 |e_u u| - \left(\alpha_3 - \frac{1}{2} k_1\right) \tanh^2(e_f) \\ & + \frac{1}{2} (\varepsilon_1 \omega_1 + \omega_2) (u^2 - u_{\hat{\tau}}^2) + \omega_1 |e_u u_{\hat{\tau}}| \\ & + \frac{\omega_3}{\hat{\tau}} \left( \hat{\tau} u^2 - \int_{t-\hat{\tau}}^t u^2(\theta) d\theta \right). \end{aligned} \tag{47}$$

**Table 2**  
Participant demographics.

Participant	Age	Sex	Condition	Time since diagnosis
S1	22	F	None	--
S2	22	M	None	--
S3	22	F	None	--
S4	22	F	None	--
S5	21	F	None	--
N1	26	M	Spina Bifida (L5-S1)	26yr
N2	55	F	Multiple Sclerosis	25yr
N3	54	M	Multiple Sclerosis	10yr
N4	42	F	Cerebral Palsy	42yr

An upper bound for (47) is obtained by following a development similar to Case 1 to yield

$$\dot{V}_L \stackrel{\text{a.e.}}{\leq} -\frac{\delta_2}{\lambda_2} V_L, \quad (48)$$

$\forall t \in [t_n^e, t_{n+1}^m)$ , provided that  $y(t_n^e) \in \mathcal{D}$  and  $\|y(\cdot)\| < \gamma$ ,  $\forall \cdot \in [t_0, t)$ .

An upper bound across all cases (i.e.,  $\forall t \in [t_0, \infty)$ ) is obtained by using (43) and (48) to yield

$$\dot{V}_L \stackrel{\text{a.e.}}{\leq} -\lambda_3 V_L, \quad (49)$$

where  $\lambda_3 \triangleq \lambda_2^{-1} \min(\delta_1, \delta_2)$ , which can be solved to yield

$$V_L(t) \leq V_L(t_0) \exp(-\lambda_3(t - t_0)), \quad (50)$$

provided that  $y(t_n^m), y(t_n^e) \in \mathcal{D}, \forall n$ , and provided that  $\|y(\cdot)\| < \gamma$ ,  $\forall \cdot \in [t_0, t)$ . Using (32) with (50) yields the result in (34). A sufficient condition for  $y(t_n^m), y(t_n^e) \in \mathcal{D}, \forall n$ , and  $\|y(\cdot)\| < \gamma$ ,  $\forall \cdot \in [t_0, t)$  is that  $y(t_0) \in S_{\mathcal{D}}$ . From (30) and (50),  $e, r, e_u \in \mathcal{L}_{\infty}$ , and from (15) and (16),  $u, u_e \in \mathcal{L}_{\infty}$  and the remaining signals are bounded.

## 5. Experiment

Let the FES and motor controllers developed in (15) and (16), the control system developed in Allen et al. (2020d), and  $u = 0$  and  $u_e = 0$  (i.e., no control assistance) be henceforth labeled as Controllers A, B, and C, respectively. Controllers A and B both have a cadence tracking objective; however, Controller A also includes a position tracking objective in an effort to improve the cadence tracking performance.

### 5.1. Experimental testbed

A modified stationary recumbent tricycle similar to Bellman et al. (2017) was used as the experimental testbed. A Quanser QPIDe data acquisition device was used to deliver motor current and to collect signal data from the encoder. The motor and FES controllers were implemented with approximate real-time control software (Quarc, Windows 10, MATLAB/Simulink) on a computer at a sampling rate of 500 Hz.

### 5.2. Experimental methods

Experiments were performed on nine participants, including four with NCs, whose demographics are shown in Table 2. Each participant provided written informed consent approved by the University of Florida Institutional Review Board (IRB201600881). Able-bodied participants, who were blind to the desired and actual trajectory, were instructed to be a passive rider and make no volitional effort to either assist or resist the electric motor input or FES input during the experiment. The able-bodied participants were asked to provide no volitional contribution for

equal comparison and to simulate the potential lack of volitional contribution by some (e.g., spinal cord injured) patients in a clinical setting. To further examine the performance of the control methods in an alternative clinical condition (i.e., active therapy), participants with NCs were asked to pedal volitionally, and FES was added as required. Furthermore, the participants with NCs were asked to contribute to the cadence tracking objective to the best of their ability, and they were shown, exclusively, a plot of the actual and desired cadence in real-time during the experiment.

Prior to the experiments, electrodes (Axelgaard ValuTrode CF7515) were placed over the quadriceps, hamstrings, and gluteal muscle groups. The participant was seated on the cycle, and their feet were secured to the pedals using orthotic boots (Össur Rebound Air Tall). The seat of the cycle was adjusted for each participant's comfort and to ensure a minimum bend of at least 15 degrees in the knee across all angles of the crank cycle. The participant specific desired FES regions for each muscle ( $\mathcal{Q}_m$ ) were determined by recording various measurements (i.e., seat position, limb lengths, etc.) as defined in Bellman et al. (2017). The motor was then used to ramp the cycle up to 50 revolutions per minute (RPM), and open-loop stimulation was applied to one muscle group at a time. The stimulation was incrementally increased until the participant's comfort limit was determined, and this limit was recorded for each muscle group. Recall that Controllers A and B utilize saturated FES controllers, thus the comfort limits were used to inform the selection of control gains to saturate the FES input at or below each muscle's comfort limit.

During the first 20 s of an experiment the motor tracked a smooth cadence ramp from zero to  $\dot{q}_d = 50$  RPM. For the remaining 160 s (the steady-state portion of the experiment), either Controller A, B, or C was implemented and a constant desired cadence of 50 RPM was tracked. For the able-bodied participants, Controllers A and B were implemented in a random order. For the participants with NCs, a run was first performed using Controller C and then a run was performed using Controller A. Since participants with NCs provided volition, they were allowed a single practice run for each controller.

## 6. Results

### 6.1. Results from able-bodied population

The experimental results (i.e., root mean square (RMS) and peak cadence errors, motor effort, and FES effort) of the able-bodied population are summarized in Table 3 for Controllers A and B. Fig. 2 depicts a plot of the desired cadence versus the actual cadence and plots of the control inputs for Participant S1 when using either Controller A or B, which represent a typical result for the able-bodied participants. Furthermore, it was determined that on average, across each able-bodied participant, Controllers A and B applied FES to at least one muscle group during 59.7% and 62.5% of the experiment, respectively, and resulted in an average cadence tracking error of  $-0.03 \pm 1.69$  RPM and  $3.90 \pm 3.36$  RPM, respectively.

#### 6.1.1. Statistical analysis and discussion

A series of statistical tests were performed to determine the impact of each controller on the cadence tracking performance and the control inputs. The statistical tests were performed on the following measurements: RMS cadence error, peak cadence error, average motor and FES inputs, motor and FES input standard deviations, and the percent of time that FES was applied. Since only two controllers (Controllers A and B) were used on each able-bodied participant, a paired difference test was used on each measurement; however, due to the small sample size ( $n = 5$ ), the

**Table 3**  
Comparative results for the able-bodied participants during steady state operation.

Controller	Participant	RMS Cadence Error (RPM)	Peak Cadence Error (RPM) <sup>a</sup>	Motor Effort (A) <sup>b</sup>	FES Effort ( $\mu$ s) <sup>c</sup>
A	S1	1.62	6.59	1.53 $\pm$ 1.20	19.76 $\pm$ 0.80
	S2	1.99	12.76	1.71 $\pm$ 1.26	36.12 $\pm$ 2.58
	S3	1.80	10.38	1.59 $\pm$ 0.95	35.42 $\pm$ 0.44
	S4	1.68	8.16	1.68 $\pm$ 1.03	12.25 $\pm$ 2.30
	S5	1.35	9.12	1.54 $\pm$ 0.90	15.49 $\pm$ 1.43
	<b>Average</b>	<b>1.69</b>	<b>9.40</b>	<b>1.61 <math>\pm</math> 1.07</b>	<b>23.81 <math>\pm</math> 1.51</b>
B	S1	4.86	13.99	1.59 $\pm$ 1.81	36.21 $\pm$ 2.60
	S2	4.90	12.65	1.71 $\pm$ 1.80	38.57 $\pm$ 1.29
	S3	3.99	11.98	2.41 $\pm$ 2.18	67.48 $\pm$ 1.54
	S4	6.08	15.64	2.48 $\pm$ 2.61	29.17 $\pm$ 0.76
	S5	5.93	14.84	2.00 $\pm$ 2.21	23.02 $\pm$ 0.89
	<b>Average</b>	<b>5.15</b>	<b>13.82</b>	<b>2.04 <math>\pm</math> 2.12</b>	<b>38.89 <math>\pm</math> 1.41</b>

<sup>a</sup>The maximum value of  $|\dot{e}|$ .

<sup>b</sup>The average  $\pm$  standard deviation of  $|u_E|$ .

<sup>c</sup>The average  $\pm$  standard deviation of the maximum stimulation delivered to each muscle group within each FES region.

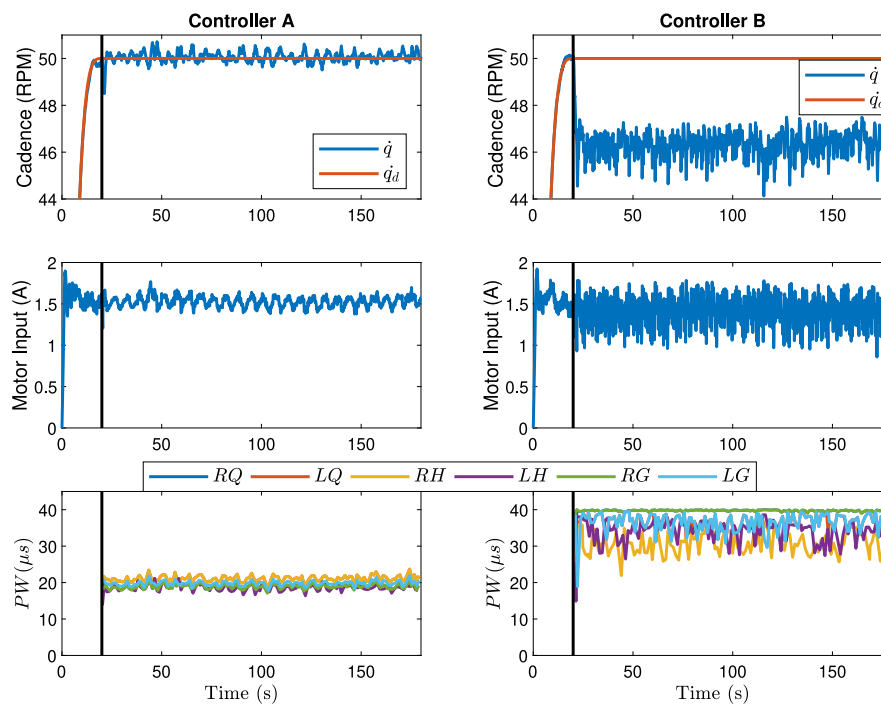


**Fig. 2.** The actual versus desired cadence after steady-state was reached (top), motor input (middle), and peak FES pulswidth (PW) input for each FES region applied to the left (L) and right (R) quadriceps (Q), hamstring (H), and gluteal (G) (bottom) are shown for Controller A (left) and Controller B (right) for participant S1. For visual clarity, a 1.2 s moving average filter was applied to the actual cadence ( $\dot{q}$ ) and the motor input. Steady-state is indicated by the vertical black line. Note that stimulation of the RG was saturated at 40  $\mu$ s, which resulted in the flat portions of the FES input for Controller B.

Shapiro–Wilk’s test for normality, whose null hypothesis is that the population is normally distributed, was used to conclude that the difference data (i.e., the difference between each controller pair for each participant) was approximately normal for each measurement (P-Value > 0.05). Therefore, a series of one-sided paired t-tests were performed to conclude that the RMS cadence error (P-Value < 0.001), peak cadence error (P-Value = 0.023), average motor effort (P-Value = 0.034), motor effort standard deviation (P-Value = 0.003), average FES effort (P-Value = 0.020), and percent of time that FES was applied (P-Value = 0.014) were significantly larger for Controller B than for Controller A. Further, it was determined that the controller had no statistically significant effect on the FES effort standard deviation (P-Value = 0.445).

From the statistical analysis and inspection of Fig. 2, it can be concluded that Controller A outperformed Controller B by reducing the cadence tracking error while simultaneously requiring

less motor and FES effort, including requiring FES to be applied over a smaller duration of time. Furthermore, it is clear from Fig. 2 that Controller B resulted in a offset of the cadence error, whereas Controller A resulted in a negligible steady-state cadence error. Controller A was developed to reduce the steady-state cadence error produced by Controller B by including a position and cadence error term in the error system. It was theorized that the position error term would act like the integral term of a Proportional–Integral–Derivative (PID) controller to reduce the steady-state error (Downey, Cheng, Bellman, & Dixon, 2017a), which was confirmed by the performance of Controller A relative to Controller B.

## 6.2. Results from population with NCs

Since Controller A outperformed Controller B, Controller B was not used on the participants with NCs and Controller C was

**Table 4**  
Comparative results for the participants with NCs during steady state operation.

Controller	Participant	RMS Cadence Error (RPM)	Peak Cadence Error (RPM) <sup>a</sup>	Motor Input (A) <sup>b</sup>	FES Input ( $\mu$ s) <sup>c</sup>
A	N1	1.98	8.86	1.29 $\pm$ 0.84	32.22 $\pm$ 1.65
	N2	1.57	7.69	1.46 $\pm$ 0.81	14.70 $\pm$ 0.53
	N3	2.19	6.72	0.93 $\pm$ 0.44	37.72 $\pm$ 6.57
	N4	2.16	7.74	1.68 $\pm$ 1.08	22.49 $\pm$ 3.31
	<b>Average</b>	<b>1.98</b>	<b>7.75</b>	<b>1.34 <math>\pm</math> 0.79</b>	<b>26.78 <math>\pm</math> 3.01</b>
C	N1	4.53	27.94	0.00 $\pm$ 0.00	0.00 $\pm$ 0.00
	N2	3.39	24.36	0.00 $\pm$ 0.00	0.00 $\pm$ 0.00
	N3	2.62	14.18	0.00 $\pm$ 0.00	0.00 $\pm$ 0.00
	N4	3.62	14.08	0.00 $\pm$ 0.00	0.00 $\pm$ 0.00
	<b>Average</b>	<b>3.54</b>	<b>20.14</b>	<b>0.00 <math>\pm</math> 0.00</b>	<b>0.00 <math>\pm</math> 0.00</b>

<sup>a</sup>The maximum value of  $|\dot{e}|$ .

<sup>b</sup>The average  $\pm$  standard deviation of  $|u_E|$ .

<sup>c</sup>The average  $\pm$  standard deviation of the maximum stimulation delivered to each muscle group within each FES region.

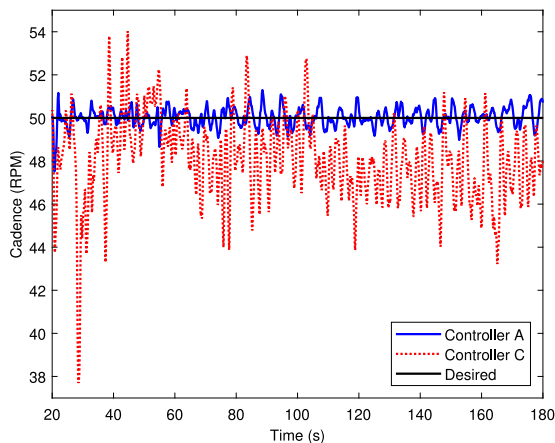


**Fig. 3.** The filtered cadence tracking results for participant N1 are shown for Controllers A (blue solid) and C (red dotted), where a 1.2 s moving average filter was applied for visual clarity. (For interpretation of the references to colour in this figure legend, the reader is referred to the web version of this article.)

instead used for comparison. The experimental results for the population with NCs are summarized in Table 4 for Controllers A and C. The cadence tracking results for Controllers A and C are depicted in Fig. 3 for Participant N1, which represents a typical result for the participants with NCs. Across each participant with NCs, it was also determined that Controllers A and C resulted in an average cadence tracking error of  $-0.04 \pm 1.98$  RPM and  $0.53 \pm 3.37$  RPM, respectively, and that, for Controller A, FES was applied to at least one muscle group during 57.4% of the experiment.

### 6.2.1. Statistical analysis and discussion

To compare the cadence tracking performance of Controllers A and C, statistical tests were performed on the RMS and peak cadence errors. As was done for the results of the able-bodied participants, normality was confirmed using the Shapiro–Wilk’s test and then one-sided paired t-tests were performed to conclude that the RMS (P-Value = 0.019) and peak (P-Value = 0.015) cadence errors were significantly larger for Controller C than Controller A.

The statistical analysis confirms that Controller A improves the cadence tracking performance relative to Controller C, which is expected since Controller C provides no control assistance to meet the control objectives. Furthermore, the experimental results in Table 4 and Fig. 3 demonstrate the cadence tracking capability of Controller A despite the existence of an unknown

time-varying EMD, presence of volitional effort from participants with a wide range of NCs, unknown disturbances, and uncertainty in the lower limb dynamics. Therefore, Controller A has demonstrated potential as a cadence tracking controller that saturates the FES input and is robust to a range of uncertainties, which can safely be used during both passive and active therapy exercises.

## 7. Conclusion

In this work, the safety/comfort and tracking performance of a participant during FES-cycling is improved by the development of a switched and saturated FES control system that is robust to uncertainties in the dynamic model, unknown disturbances, and an unknown time-varying EMD. Exponential position and cadence tracking are guaranteed by a Lyapunov-based stability analysis. An important feature of the control system is that the bound on the FES controller can be set a priori to be within the tolerable range of the participant to ensure comfort. Furthermore, state and delay dependent switching conditions were developed to properly activate/deactivate the motor and the FES of each muscle group to ensure efficient muscle contractions.

A series of experiments were performed on five able-bodied participants and four participants with NCs to validate the performance of the developed controller. For able-bodied participants, the developed controller and the controller in Allen et al. (2020d) resulted in an average cadence tracking error of  $-0.03 \pm 1.69$  RPM and  $3.90 \pm 3.36$  RPM, respectively. Likewise, the developed controller produced an average cadence tracking error of  $-0.04 \pm 1.98$  RPM for the participants with NCs. Future efforts include the development of an adaptive and saturated FES controller to better adapt to each individual participant, while ensuring participant comfort.

## Acknowledgments

This research is supported in part by NSF, USA Award number 1762829, the Assistant Secretary of Defense for Health Affairs, through the Congressionally Directed Medical Research Program under Award No. W81XWH1910330, and the National Defense Science and Engineering Graduate, USA Fellowship Program. Any opinions, findings and conclusions or recommendations expressed in this material are those of the author(s) and do not necessarily reflect the views of the sponsoring agency.

## References

- Allen, B., Cousin, C., Rouse, C., & Dixon, W. E. (2019a). Cadence tracking for switched FES-cycling with unknown time-varying input delay. In *Proc. ASME dyn. syst. control conf.*

- Allen, B. C., Cousin, C., Rouse, C., & Dixon, W. E. (2019b). Cadence tracking for switched FES cycling with unknown input delay. In *Proc. IEEE conf. decis. control* (pp. 60–65). Nice, Fr.
- Allen, B. C., Cousin, C. A., Rouse, C. A., & Dixon, W. E. (2022). Robust cadence tracking for switched FES-cycling with an unknown time-varying input delay. *IEEE Transactions on Control Systems Technology*, 30(2), 827–834.
- Allen, B. C., Stubbs, K. J., & Dixon, W. E. (2020a). Characterization of the time-varying nature of electromechanical delay during FES-cycling. *IEEE Transactions on Neural Systems and Rehabilitation Engineering*, 28(10), 2236–2245.
- Allen, B. C., Stubbs, K., & Dixon, W. E. (2020b). Robust cadence tracking for switched FES-cycling with an unknown time-varying input delay using a time-varying estimate. In *IFAC world Congr.*
- Allen, B. C., Stubbs, K., & Dixon, W. E. (2020c). Robust power and cadence tracking on a motorized FES cycle with an unknown time-varying input delay. In *Proc. IEEE conf. decis. control* (pp. 3407–3412).
- Allen, B. C., Stubbs, K. J., & Dixon, W. E. (2020d). Saturated control of a switched FES-cycle with an unknown time-varying input delay. In *IFAC conf. cyber-phys. hum.-syst.*
- Allen, B. C., Stubbs, K. J., & Dixon, W. E. (2021). Electromechanical delay during functional electrical stimulation induced cycling is a function of lower limb position. *Disability and Rehabilitation: Assistive Technology*, 1–6.
- Bagheri, M., Naseradinmousavi, P., & Krstic, M. (2019). Feedback linearization based predictor for time delay control of a high-DOF robot manipulator. *Automatica*, 108.
- Bellman, M. J., Downey, R. J., Parikh, A., & Dixon, W. E. (2017). Automatic control of cycling induced by functional electrical stimulation with electric motor assistance. *IEEE Transactions on Automation Science and Engineering*, 14(2), 1225–1234.
- Cousin, C. A., Rouse, C. A., Duenas, V. H., & Dixon, W. E. (2019). Controlling the cadence and admittance of a functional electrical stimulation cycle. *IEEE Transactions on Neural Systems and Rehabilitation Engineering*, 27(6), 1181–1192.
- Downey, R. J., Cheng, T.-H., Bellman, M. J., & Dixon, W. E. (2017a). Switched tracking control of the lower limb during asynchronous neuromuscular electrical stimulation: Theory and experiments. *IEEE Transactions on Cybernetics*, 47(5), 1251–1262.
- Downey, R., Merad, M., Gonzalez, E., & Dixon, W. E. (2017b). The time-varying nature of electromechanical delay and muscle control effectiveness in response to stimulation-induced fatigue. *IEEE Transactions on Neural Systems and Rehabilitation Engineering*, 25(9), 1397–1408.
- Ferrante, S., Pedrocchi, A., Ferrigno, G., & Molteni, F. (2008). Cycling induced by functional electrical stimulation improves the muscular strength and the motor control of individuals with post-acute stroke. *European Journal of Physical and Rehabilitation Medicine*, 44(2), 159–167.
- Filippov, A. F. (1964). Differential equations with discontinuous right-hand side. In *American mathematical society translations - Series 2: vol. 42, Fifteen papers on differential equations* (pp. 199–231). American Mathematical Society.
- Fischer, N., Dani, A., Sharma, N., & Dixon, W. E. (2013a). Saturated control of an uncertain nonlinear system with input delay. *Automatica*, 49(6), 1741–1747.
- Fischer, N., Kamalapurkar, R., & Dixon, W. E. (2013b). Lasalle-yoshizawa corollaries for nonsmooth systems. *IEEE Transactions on Automatic Control*, 58(9), 2333–2338.
- Hooker, S. P., Figoni, S. F., Rodgers, M. M., Glaser, R. M., Mathews, T., Suryaprasad, A. G., et al. (1992). Physiologic effects of electrical stimulation leg cycle exercise training in spinal cord injured persons. *Archives of Physical Medicine and Rehabilitation*, 73(5), 470–476.
- Karafyllis, L., & Krstic, M. (2017). *Predictor feedback for delay systems: implementations and approximations*. Springer.
- Karafyllis, L., Malisoff, M., de Queiroz, M., Krstic, M., & Yang, R. (2015). Predictor-based tracking for neuromuscular electrical stimulation. *International Journal of Robust and Nonlinear*, 25(14), 2391–2419.
- Krstic, M. (2009). *Delay compensation for nonlinear, adaptive, and PDE systems*. Springer.
- Krstic, M. (2010). Input delay compensation for forward complete and strict-feedforward nonlinear systems. *IEEE Transactions on Automatic Control*, 55, 287–303.
- Mazenc, F., & Malisoff, M. (2020). Continuous discrete sequential observers for time-varying systems under sampling and input delays. *IEEE Transactions on Automatic Control*, 65(4), 1704–1709.
- Mazenc, F., Malisoff, M., & Ozbay, H. (2018). Stability and robustness analysis for switched systems with time-varying delays. *SIAM Journal on Control and Optimization*, 56, 158–182.
- Mazenc, F., Mondie, S., Francisco, R., Conge, P., Lorraine, I., & Metz, F. (2004). Global asymptotic stabilization of feedforward systems with delay in the input. *IEEE Transactions on Automatic Control*, 49, (5), 844–850.
- Merad, M., Downey, R. J., Obuz, S., & Dixon, W. E. (2016). Isometric torque control for neuromuscular electrical stimulation with time-varying input delay. *IEEE Transactions on Control Systems Technology*, 24(3), 971–978.
- Nordez, A., Gallot, T., Catheline, S., Guével, A., Cornu, C., & Hug, F. (2009). Electromechanical delay revisited using very high frame rate ultrasound. *Journal of Applied Physiology*, 106, 1970–1975.
- Obuz, S., Duenas, V. H., Downey, R. J., Klotz, J. R., & Dixon, W. E. (2020). Closed-loop neuromuscular electrical stimulation method provides robustness to unknown time-varying input delay in muscle dynamics. *IEEE Transactions on Control Systems Technology*, 28(6), 2482–2489.
- Oliveira, T. R., Costa, L. R., Pino, A. V., & Paz, P. (2019). Extremum seeking-based adaptive PID control applied to neuromuscular electrical stimulation. *Anais da Academia Brasileira de Ciências*, 91.
- Paden, B. E., & Sastry, S. S. (1987). A calculus for computing Filippov's differential inclusion with application to the variable structure control of robot manipulators. *IEEE Transactions on Circuits and Systems*, 34(1), 73–82.
- Paz, P., Oliveira, T. R., Pino, A. V., & Fontana, A. P. (2020). Model-free neuromuscular electrical stimulation by stochastic extremum seeking. *IEEE Transactions on Control Systems Technology*, 28(1), 238–253.
- Pons, D. J., Vaughan, C. L., & Jaros, G. G. (1989). Cycling device powered by the electrically stimulated muscles of paraplegics. *Medical & Biological Engineering & Computing*, 27(1), 1–7.
- Schutte, L. M., Rodgers, M. M., Zajac, F. E., & Glaser, R. M. (1993). Improving the efficacy of electrical stimulation-induced leg cycle ergometry: An analysis based on a dynamic musculoskeletal model. *IEEE Transactions on Rehabilitation Engineering*, 1(2), 109–125.
- Sharma, N., Gregory, C., & Dixon, W. E. (2011). Predictor-based compensation for electromechanical delay during neuromuscular electrical stimulation. *IEEE Transactions on Neural Systems and Rehabilitation Engineering*, 19(6), 601–611.
- Wang, Y., Niu, B., Wu, B., & Xie, X. (2018). Asynchronous switching for switched nonlinear input delay systems with unstable subsystems. *Journal of the Franklin Institute*, 355, 2912–2931.
- Wang, Y., Sun, X., & Mazenc, F. (2016). Stability of switched nonlinear systems with delay and disturbance. *Automatica*, 69.
- Yang, D., Li, X., & Qiu, J. (2019). Output tracking control of delayed switched systems via state-dependent switching and dynamic output feedback. *Nonlinear Analysis: Hybrid Systems*, 32, 294–305.
- Zhou, B., & Lin, Z. (2011). Parametric Lyapunov equation approach to stabilization of discrete-time systems with input delay and saturation. *IEEE Transactions on Circuits and Systems I: Regular Papers*, 58(11), 2741–2754.
- Zhou, B., Lin, Z., & Duan, G. (2010). Stabilization of linear systems with input delay and saturation - a parametric Lyapunov equation approach. *International Journal of Robust and Nonlinear Control*, 20(13), 1502–1519.
- Zhou, Q., Wu, C., & Shi, P. (2017). Observer-based adaptive fuzzy tracking control of nonlinear systems with time delay and input saturation. *Fuzzy Sets and Systems*, 316, 49–68.



**Brendon C. Allen** received his Ph.D. in mechanical engineering from the University of Florida in 2021. He subsequently joined the Department of Mechanical Engineering at Auburn University as a faculty member in August 2021. In 2019, he was awarded a National Defense Science and Engineering Graduate Fellowship. His research interests include nonlinear and adaptive control of uncertain nonlinear systems, rehabilitation engineering, hybrid exoskeletons, and autonomous systems.



**Kimberly J. Stubbs** earned her Bachelor of Science degree in Mechanical Engineering in May 2019 and her Master of Science degree in Mechanical Engineering in May 2021, both from the University of Florida. She is the recipient of a Graduate School Preeminence Award fellowship, awarded in August 2019. Kimberly has participated in the development of several rehabilitative robotics devices, including an isokinetic cycling system for children with Duchenne Muscular Dystrophy and a teleoperated FES-enabled cycling system for people with neurological conditions. She is currently pursuing

a Ph.D. under the supervision of Dr. Warren Dixon. Kimberly's research interests are primarily focused on human-robot interaction and rehabilitative robotics. Expected graduation is May 2023.



**Warren E. Dixon** received his Ph.D. in 2000 from the Department of Electrical and Computer Engineering from Clemson University. He was selected as a Eugene P. Wigner Fellow and worked as a staff researcher at Oak Ridge National Laboratory. In 2004, he joined the University of Florida in the Mechanical and Aerospace Engineering Department, where he is currently serving as the Dean's Leadership Professor and Department Chair. His main research interest has been the development and application of Lyapunov-based control techniques for uncertain nonlinear systems. His work

has been acknowledged by various career and best paper awards, and he attained ASME and IEEE Fellow for contributions to adaptive control of uncertain nonlinear systems.